Kovove Mater. 64 2026 161–171
DOI: 10.31577/km.2026.3.161

Microstructural recovery and stored energy in API 5L X70 steel during low-temperature annealing: XRD, SEM, and computational study

Safa Abderrahmani[1]*, Nedjema Chérifi[2], Kenza Ghanem[3]

[1]*Department of Chemical Engineering, Science and Technology Faculty, University of Biskra, BP 145 RP, Biskra 07000, Algeria*
[2]*Laboratory of GPCE, Science and Technology Faculty, University of Biskra, BP 145 RP, Biskra 07000, Algeria*
[3]*Laboratory of LARGHYDE, Science and Technology Faculty, University of Biskra, BP 145 RP, Biskra 07000, Algeria*

Received 9 April 2026, received in revised form 8 May 2026, accepted 18 June 2026

Abstract

This work examines the microstructural and mechanical response of API 5L X70 pipeline steel subjected to low-temperature isothermal annealing at 200 °C for 4 hours. Unlike conventional high-temperature treatments that often cause grain coarsening, this study focuses on the effects of a mild thermal cycle on the material's internal energy using a multi-scale analytical approach. Williamson-Hall X-ray diffraction (XRD), scanning electron microscopy (SEM), and computational image analysis were employed to quantify recovery mechanisms.

Results indicate that annealing at 200 °C significantly reduces lattice microstrain (from $\varepsilon = 6.53 \times 10^{-4}$ to 0.19×10^{-4}), primarily through dislocation rearrangement and partial annihilation rather than full recrystallization. The stored energy decreases substantially from 0.313 to 0.014 MJ m^{-3}. SEM-based quantitative analysis shows a more homogeneous microstructure, with the number of detected sub-grain features rising from 2.533 to 10,485 and the mean projected area decreasing by roughly 75 %. Despite these structural modifications, the steel maintains its mechanical integrity, with Vickers hardness decreasing moderately to 208.22 HV. Overall, annealing at 200 °C efficiently relieves residual stresses while preserving structural stability and load-bearing capacity. The integrated experimental and computational framework presented here provides a reliable methodology for evaluating recovery mechanisms and their influence on the performance of X70 pipeline steel.

K e y w o r d s: API 5L X70 steel, low-temperature annealing, microstrain relaxation, static recovery, stored energy, microstructural homogenization

Introduction

The operational safety and long-term performance of high-pressure energy infrastructure are closely related to the microstructural state of high-strength low-alloy (HSLA) steels. Achieving a balance between mechanical strength, fracture resistance, and service reliability remains a challenge, particularly under increasingly demanding operating conditions. In this context, API 5L X70 steel is widely used for oil and gas transmission pipelines due to its high yield strength, good weldability, and stable performance, including at relatively low temperatures [1, 2]. Its microstructure typically consists of a fine-grained ferritic-pearlitic matrix, with possible contributions from bainitic or acicular ferrite phases depending on thermo-mechanical controlled processing (TMCP) and cooling conditions, which are used to adjust ductility and toughness [2].

In industrial applications, thermal treatments are commonly applied to reduce residual stresses, modify sub-grain structures, and promote the rearrangement of dislocations. These changes contribute to improving resistance to fatigue, stress-corrosion cracking, and degradation under high-pressure service conditions [4–6]. In addition, appropriate heat treatments can extend the service life of pipelines and maintain struc-

*Corresponding author: e-mail address: safa.abderrahmani@univ-biskra.dz

tural stability over long periods [7–9].While the effects of high-temperature annealing are well documented, the behavior of materials subjected to lower temperature treatments remains less extensively reported. Annealing in the range of 200–350 ℃ is of particular interest, as it can promote recovery processes and reduce dislocation density without inducing significant phase transformations or grain growth [5].

To address this gap, the present study focuses on the microstructural and mechanical response of API 5L X70 steel subjected to isothermal annealing at 200 ℃ for 4 hours. The study adopts a multi-scale experimental framework combining X-ray diffraction (XRD), scanning electron microscopy (SEM), and quantitative image analysis to capture the material behavior across different length scales. In parallel, computational tools are employed to estimate key parameters such as stored energy, thereby supporting a more consistent interpretation of the experimental observations. Overall, this integrated approach enables a quantitative description of the recovery process and its influence on both microstructural uniformity and mechanical response, contributing to a deeper understanding of the effects of low-temperature annealing on pipeline steels.

2. Experimental material and techniques

2.1. Material and specimen preparation

The material investigated in this study is API 5L X70 high-strength low-alloy (HSLA) pipeline steel, obtained from an in-service section provided by Cosider Company (Biskra, Algeria). To preserve the initial thermomechanical condition and avoid thermal alteration during cutting, specimens ($15 \times 22\,\mathrm{mm}^2$) were sectioned using a precision cold saw under continuous lubrication. The nominal chemical composition and baseline mechanical properties, as provided by the manufacturer for this batch, are presented in Tables 1 and 2 to ensure reproducibility.

2.2. Isothermal annealing protocol

Selected specimens were subjected to isothermal annealing at 200 ℃ for 4 h in a Nabertherm B180 laboratory furnace. To ensure uniform thermal exposure, the samples were placed in the furnace only after it reached the target temperature. After annealing, they were cooled naturally to room temperature to reduce thermal gradients and avoid the introduction of additional residual stresses.

The use of a single annealing temperature (200 ℃) was intentional in order to isolate the effect of static recovery on dislocation rearrangement, while avoiding phase transformations and recrystallization. This temperature is representative of low thermal exposure conditions relevant to industrial processing and service environments in API 5L X70 steel. This approach enables a focused analysis of the early stages of microstructural evolution and stored energy reduction. Further work will consider a wider temperature range to investigate the transition toward recrystallization.

2.3. Metallographic and microstructural characterization

Specimens were prepared using standard metallographic procedures. Grinding was carried out with silicon carbide (SiC) papers (80–4000 grit) under continuous water lubrication, followed by polishing with diamond suspensions down to 1 μm to obtain a mirror-like surface. The ferritic-pearlitic microstructure was revealed by etching with a 2% Nital solution for 14 s.

Microstructural observations were performed using scanning electron microscopy (SEM) at an accelerating voltage of 20 kV. Crystallographic characterization was conducted by X-ray diffraction (XRD) using Cu-Kα radiation ($\lambda = 1.5406$ Å), over a 2θ range of 30°–100° with a step size of 0.02°. These conditions allow the application of the Williamson-Hall (W-H) method to separate the contributions of crystallite size and lattice strain to peak broadening. Although techniques such as transmission electron microscopy (TEM) or electron backscatter diffraction (EBSD) provide higher spatial resolution, the combined use of SEM and XRD in this study enables a representative, non-destructive evaluation of the material at different scales.

2.4. Mechanical evaluation and computational analysis

Mechanical properties were assessed using Vickers hardness testing under a load of 10 kgf (HV10) with a dwell time of 10 s. Thirty indentations were performed for each condition to ensure statistical reliability, and average values were calculated.

To support the interpretation of the experimental results, a computational framework was used to combine data obtained at different scales. This approach included:

– *Morphological analysis*: SEM images were processed to quantify microstructural feature distributions and their projected areas.

– *Crystallographic evaluation*: Lattice microstrain (ε) and dislocation density (ρ) were determined using the Williamson-Hall method.

– *Statistical analysis*: Radar plots and Pearson correlation matrices were used to examine relationships between microstructural parameters and mechanical response.

This combined experimental and computational

Table 1. Chemical composition of X70 pipeline steel (mass fraction, %) [6]

C	Mn	Ti	Nb	S	P	Si	Mo	Cu	Fe
0.041	1.76	0.023	0.067	0.006	0.016	0.281	0.194	0.193	Balance

Table 2. Mechanical properties of X70 pipeline steel [6]

Yield strength (MPa)	Ultimate tensile strength (MPa)	Elongation (%)	Reduction in area (%)
583	660	20.3	78.7

Table 3. Williamson-Hall plotting parameters of X70 steel (As-Received and Heat-treated 200 ℃, 4 h)

Pic	Pos. [2θ]	FWHM Left [2θ]	4 sinθ (X)	β_L cosθ (Y)	Microstrain, ε ($\times 10^{-4}$)	Crystallite size, D (nm)	Dislocation density, ρ ($\times 10^{-4}$ nm^{-2})
X70-AsR							
1	40.1731	0.0886	1.374	0.00145			
2	44.6409	0.2362	1.519	0.00381			
3	64.8290	0.3247	2.144	0.00478	6.53	71.64	1.274
4	82.2663	0.2880	2.631	0.00379			
5	98.8602	0.2880	3.038	0.00327			
Heat-treated sample (T = 200 ℃, t = 4 h)							
1	40.0960	0.1771	1.371	0.00290			
2	44.6104	0.1771	1.518	0.00286			
3	64.8337	0.2362	2.144	0.00348	0.19	47.82	0.055
4	82.2290	0.2160	2.630	0.00284			
5	98.7758	0.2520	3.037	0.00286			

approach provides a consistent basis for analyzing recovery behavior, changes in lattice structure, and their influence on the mechanical properties of API 5L X70 steel after low-temperature annealing.

Table 1 summarizes the chemical composition of the investigated API 5L X70 steel, corresponding to a low-carbon microalloyed system. The baseline mechanical properties of the as-received material, including a yield strength of 583 MPa and an elongation of 20.3 %, are presented in Table 2.

3. Experimental results and discussion

This section presents the experimental results obtained from X-ray diffraction (XRD), scanning electron microscopy (SEM), automated particle analysis, and Vickers microhardness (HV) measurements. The analysis focuses on the evolution of the microstructure and mechanical behavior of API 5L X70 steel in the as-received condition and after isothermal annealing at 200 ℃ for 4 hours.

3.1. X-ray diffraction analysis and crystallographic parameters

The main crystallographic parameters derived from the XRD patterns are summarized in Table 3. Diffraction peak positions (2θ) and full widths at half maximum (FWHM) were determined using HighScore software and used as input for the Williamson-Hall (W-H) analysis. This method allows the separation of peak broadening contributions associated with crystallite size and lattice strain.

W-H plots (Fig. 1) were constructed using linear regression. In this approach, the lattice microstrain (ε) is obtained from the slope, while the crystallite size (D) is derived from the intercept. The dislocation density (ρ) was then estimated from these parameters, providing an indication of the defect content within the lattice. The results are summarized in Table 3 and form the basis for analyzing the structural evolution of the material [7].

For each diffraction peak, the W-H variables were calculated as follows:

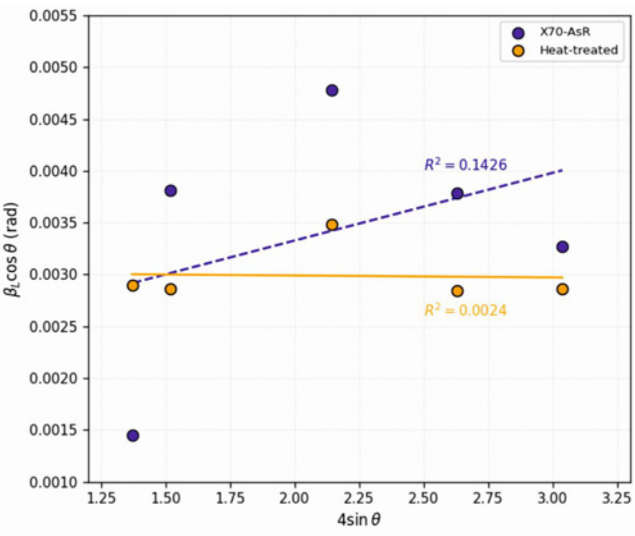

Fig. 1. Williamson-Hall plots of API 5L X70 steel before and after heat treatment at 200 °C for 4 hours.

$$X = 4 \times \sin(\theta), \quad (1)$$

$$Y = \beta_{\mathrm{L}} \times \cos(\theta), \quad (2)$$

where θ is the Bragg angle and β_{L} is the FWHM corrected for instrumental broadening. Linear regression of Y as a function of X allows the determination of D and ε from the intercept and slope, respectively [8].

The crystallite size was also estimated using the Scherrer equation (Eq.(3)):

$$D = \frac{K \times \lambda}{\beta_{\mathrm{L}} \cos\theta}, \quad (3)$$

where K is the shape factor (0.94) and λ is the Cu Kα wavelength (0.154 nm). The lattice microstrain (ε) reflects elastic distortions within the crystal lattice and is obtained from the slope of the W-H plot.

The dislocation density (ρ), which represents the concentration of line defects, was calculated using the Williamson-Smallman relation [9, 10]:

$$\rho = \frac{2\sqrt{3}}{Db}\varepsilon^2, \quad (4)$$

where b is the Burgers vector (0.248 nm), corresponding to the {111} and {110} slip systems in BCC ferrite [12].

This approach provides a consistent framework for following changes in lattice strain, crystallite size, and defect density during low-temperature annealing.

Table 3 presents the crystallographic parameters obtained from the Williamson-Hall (W-H) analysis, including the full width at half maximum (FWHM), lattice microstrain (ε), and dislocation density (ρ) for both the as-received and heat-treated samples.

The crystallographic evolution of API 5L X70 steel was analyzed using the W-H method, with the results presented in Fig. 1 and summarized in Table 3. In the as-received (AsR) condition, the W-H plot shows a positive slope ($R^2 = 0.1426$), indicating a relatively high lattice microstrain ($\varepsilon = 6.53 \times 10^{-4}$). This value reflects the presence of lattice distortions and internal stresses introduced during thermomechanical controlled processing (TMCP) [8, 13–16]. These features are associated with a relatively high dislocation density ($\rho = 1.274 \times 10^{-4}\,\mathrm{nm}^{-2}$) within the ferritic matrix. The calculated crystallite size ($D = 71.64\,\mathrm{nm}$) corresponds to coherent diffracting domains, which are subdivided by dislocation structures rather than representing actual grain boundaries.

After isothermal annealing at 200 °C for 4 hours, the W-H plot becomes nearly horizontal ($R^2 = 0.0024$), indicating a strong reduction in lattice microstrain ($\varepsilon = 0.19 \times 10^{-4}$). This change is consistent with recovery processes, where thermal activation promotes dislocation rearrangement and partial annihilation, leading to a decrease in internal stresses. As a result, the dislocation density decreases to $0.055 \times 10^{-4}\,\mathrm{nm}^{-2}$. The reduction in crystallite size to 47.82 nm should not be interpreted as grain refinement; rather, it is related to the reorganization of coherent diffraction domains and to the lower sensitivity of the W-H method when the strain contribution becomes small. This apparent decrease is attributed to the progressive relaxation and fragmentation of coherent diffraction domains under strain relief.

In addition, the decrease in FWHM values for all diffraction peaks (Table 3) suggests that peak broadening in the annealed condition is less affected by lattice strain and more associated with the stabilization of substructures. This behavior is consistent with a recovery-controlled mechanism in ferritic microalloyed steels [16–19].

3.2. SEM microstructural observations

The SEM micrographs of the as-received (AsR) API 5L X70 steel (Fig. 2a) show a ferritic matrix with fragmented pearlitic colonies. The ferritic grains display irregular shapes and a wide size distribution, reflecting the effects of thermomechanical controlled processing (TMCP) and subsequent cooling. This heterogeneous structure is consistent with the relatively high lattice microstrain ($\varepsilon = 6.53 \times 10^{-4}$) obtained from the Williamson-Hall analysis. In addition, contrast variations and the slightly diffuse appearance within the grains suggest the presence of a high density of substructural defects, such as dislocation tangles ($\rho = 1.274 \times 10^{-4}\,\mathrm{nm}^{-2}$) and localized lattice distortions [8, 13, 21]. These observations indicate

Table 4. Quantitative analysis of SEM-based microstructural features in X70 steel before and after heat treatment at 200 °C for 4 hours

Samples	Number of detected features	Feature density (features/mm^2)	Mean projected area (µm^2)
X70-AsR	2533	0.02157	46.44
X70-200 °C-4 h	10485	0.08927	11.22

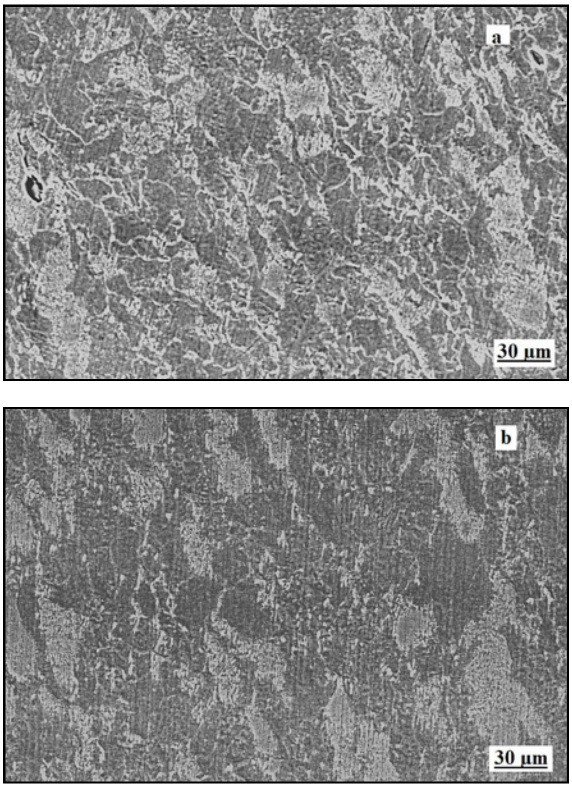

Fig. 2. SEM micrographs of the experimental X70 steel; (a) the untreated sample and (b) the specimen subjected to heat treatment at 200 °C for 4 hours.

that peak broadening in the as-received condition is mainly influenced by lattice strain. Accordingly, the crystallite size obtained from the W-H method (D = 71.64 nm) corresponds to coherent diffracting domains within larger grains, rather than the actual grain size.

After annealing at 200 °C for 4 hours (Fig. 2b), the microstructure appears more uniform. Ferritic grains are more clearly defined, with sharper boundaries and reduced internal contrast, in agreement with the decrease in lattice microstrain ($\varepsilon = 0.19 \times 10^{-4}$). This change is consistent with a recovery process, where thermal activation promotes dislocation rearrangement and partial annihilation, leading to a reduction in internal stresses. The dislocation density decreases accordingly to 0.055×10^{-4} nm^{-2}.

Some faint linear features aligned with the rolling direction (RD) remain visible, indicating that the initial thermomechanical history is not completely removed. This suggests that annealing at 200 °C promotes recovery mechanisms without any occurrence of recrystallization or significant grain growth [16, 17]. The material therefore remains in a recovery-dominated state, where defect rearrangement reduces stored energy while preserving the overall grain structure. In this context, the reduction in crystallite size to 47.82 nm is attributed to the redistribution and stabilization of coherent domains rather than to actual grain refinement.

3.3. Microstructural feature analysis and quantification

To quantify microstructural changes, digital image analysis was performed using *Mountains Software* (based on SPIP^{TM} technology). This approach enables the identification and quantification of microstructural features, including grains, sub-boundaries, and coherent domains, through advanced image segmentation techniques. A combination of ISO 25178-2 watershed segmentation and threshold-based segmentation was applied to extract key geometrical parameters from SEM images. These parameters include the mean projected area, feature density, and equivalent diameter (Table 4), all expressed as image-based measurements derived from SEM micrographs. Pseudo-color overlays (Fig. 3) were additionally used to visualize microstructural homogenization and the redistribution of domains during the recovery process at 200 °C.

Figure 3 and Table 4 illustrate the evolution of microstructural features in X70 steel following annealing. The SEM observations (Fig. 3b) reveal a more homogeneous and refined microstructure, in agreement with the quantitative results presented in Table 4. The observed increase in feature density, accompanied by a decrease in mean projected area, indicates a progressive subdivision of the microstructure into smaller and more uniformly distributed domains. This evolution is mainly attributed to dislocation rearrangement and the formation of stable sub-boundaries during annealing at 200 °C, rather than precipitation or physical fragmentation.

To correlate SEM observations with crystallographic data, automated image analysis was performed, providing a quantitative description of the microstructural evolution (Table 4, Fig. 3). In the as-received (AsR) condition, the material exhibits

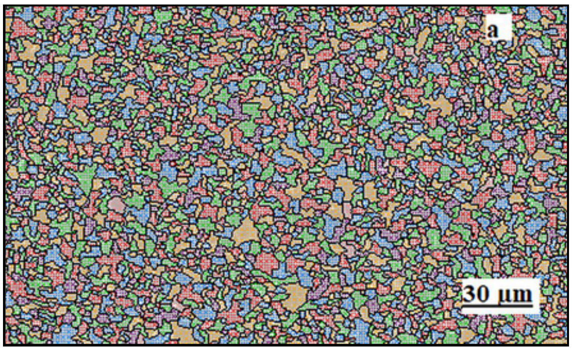

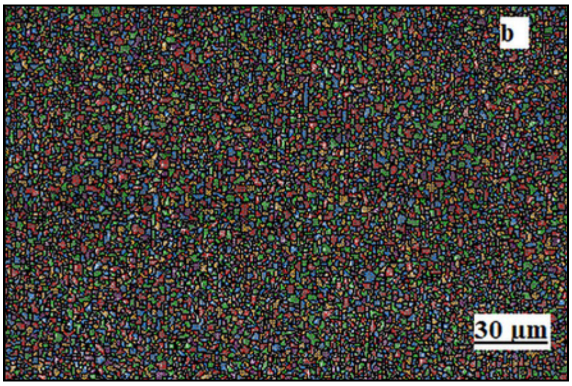

Fig. 3. Microstructural feature analysis based on SEM images of X70 steel: (a) as-received sample and (b) sample heat-treated at 200 °C for 4 hours.

a coarse and heterogeneous morphology, with 2,533 detected features and a mean projected area of 46.44 μm^2. This is consistent with the relatively high lattice microstrain and dislocation density obtained from Williamson–Hall analysis. The difference between the micrometer-scale features observed by SEM and the nanometric crystallite size ($D = 71.64$ nm) reflects the hierarchical nature of the microstructure, where ferritic grains contain multiple strain-affected coherent domains.

After annealing at 200 °C, the microstructure becomes more uniform. The number of detected features increases to 10,485, while the mean projected area decreases to 11.22 μm^2. This apparent refinement does not correspond to grain fragmentation, but rather to the rearrangement of dislocations into more stable, low-energy sub-boundaries, which are identified as distinct features in the image analysis. These observations are consistent with the reduction in microstrain and dislocation density obtained from XRD measurements. Overall, the results indicate that the microstructural evolution is governed by recovery mechanisms, where defect rearrangement reduces stored energy without altering the phase structure. The improved homogeneity and clearer grain interiors observed in SEM further support this conclusion [17].

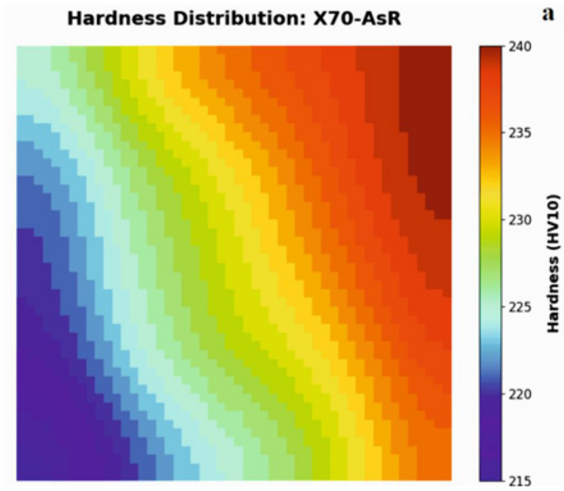

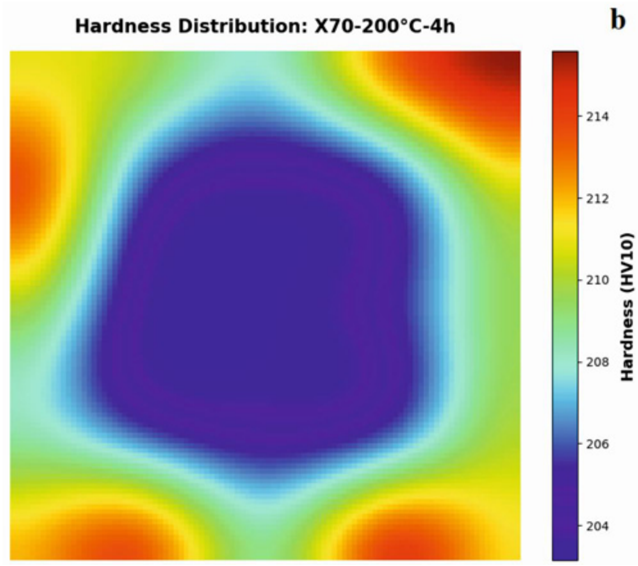

Fig. 4. Color hardness maps of X70 steel: (a) untreated sample and (b) sample after heat treatment at 200 °C for 4 hours.

3.4. Microhardness evaluation and statistical mapping

The mechanical response of X70 steel was assessed using Vickers hardness testing with a Falcon automated system. Indentations were performed under a 10 kgf load (HV10) with a dwell time of 10 s. More than 30 measurements were taken for each condition to ensure statistical reliability. Hardness distribution across the sample surfaces was visualized using color contour maps (Figs. 4a,b), providing insight into mechanical uniformity. Complementary hardness profiles are shown in Figs. 5a,b, while the corresponding mean values and standard deviations are summarized in Table 5.

The mechanical behavior of API 5L X70 steel, assessed through Vickers hardness measurements (Ta-

Table 5: Summary of Vickers hardness values for X70 steel before and after heat treatment

Samples	Mean HV	Min HV	Max HV	Standard deviation (SD)
X70-AsR	225.43	215.16	239.70	6.45
X70-200 ℃-4 h	208.22	203.14	215.58	3.50

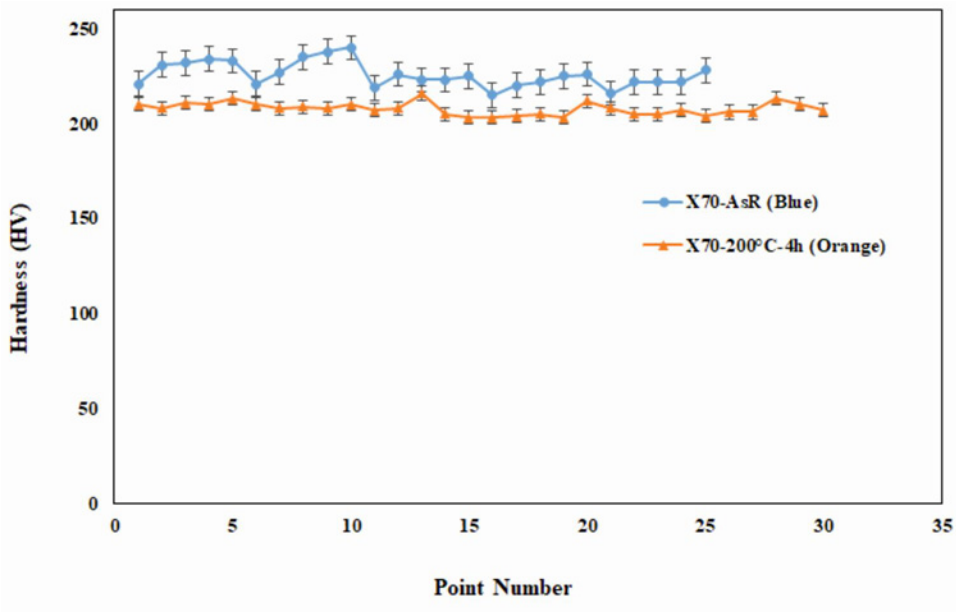

Fig. 5. Vickers hardness profiles of API 5L X70 steel in the as-received (AsR) condition and after heat treatment at 200 ℃ for 4 hours.

ble 5; Figs. 4 and 5), aligns well with the microstructural changes observed by XRD and SEM. In the as-received (AsR) state, the material shows a relatively high average hardness of 225.43 HV, which is primarily related to the elevated dislocation density and significant lattice microstrain identified by Williamson-Hall analysis. The presence of dense substructural defects, also reflected in the heterogeneous distribution of microstructural features and the diffuse contrast observed in SEM images, contributes to strengthening through dislocation interactions.

After annealing at 200 ℃ for 4 hours, hardness decreases moderately to 208.22 HV, with a narrower distribution ranging from 203.14 to 215.58 HV. This change reflects the relaxation of internal stresses and a reduction in dislocation density. Feature analysis confirms this trend, showing an increased number of substructural features and a more uniform microstructure due to dislocation rearrangement and partial annihilation.

These findings indicate that low-temperature annealing promotes recovery, reducing stored energy while preserving the overall structural integrity. This observation is consistent with previous reports [22, 23] which showed that annealing at moderate temperatures can relieve residual stresses without significant softening or grain coarsening typically seen at higher temperatures ($\geq$ 350 ℃) [1, 24]. While techniques such as EBSD could provide additional grain boundary details, the combination of microhardness testing, W-H analysis, SEM imaging, and quantitative feature analysis offer a coherent understanding of the link between microstructural evolution and mechanical response.

3.5. Comparison with previous studies

Benchmarking the present results against previous studies (Table 6) confirms that annealing at 200 ℃ effectively balances microstructural stability and mechanical performance. Unlike high-temperature treatments reported by Liu et al. [22] and Zhu et al. [23] which often led to grain coarsening and phase transformations, the mild thermal cycle used in this work preserves the initial structural characteristics of API 5L X70 steel. Intermediate treatments studied by Digheche et al. [1], and Mohtadi-Bonab et al. [24] sometimes showed limited or inconsistent improvements, whereas the 4-hour holding time applied in this study promotes a more uniform microstructural evolution compared to shorter durations reported by Masoumi et al. [25].

The recovery state is further supported by the

Table 6: Comparative summary of heat treatment conditions and outcomes for X70 steel reported in various studies.

Study	Heat treatment conditions	Observed effects	Main conclusion
This study	200 ℃, 4 h	Homogeneous microstructure, significantly reduced microstrain apparent decrease in coherent domain size (45.77 nm), refined microstructural feature distribution, stable hardness (208.22 HV), reduced dislocation density ($\rho = 0.055 \times 10^{-4}\,\mathrm{nm}^{-2}$)	Mild annealing effectively reduces lattice defects, enhances uniformity, and maintains mechanical stability
[22]	720–950 ℃, few min	Excessive grain growth, phase transformations, high residual stresses	High-temperature annealing reduces structural stability
[24]	350 ℃, 30 min	Minor improvement, slight loss of hardness/ductility	Limited benefits of intermediate-temperature treatment
[23]	500–550 ℃, 30 min–2 h	Grain coarsening, reduced homogeneity, partial refinement	Higher temperatures may induce undesirable structural changes
[1]	200, 400, 600 ℃, 30 min	Slight or negative effects on hardness and ductility	No consistent improvement across temperature range
[25]	1200 ℃, 60 min	Partial stress relief, less uniform microstructure	Short exposure at high temperature insufficient for full recovery

agreement between SEM observations and Williamson-Hall XRD results. The substantial reduction in lattice microstrain and the decrease in dislocation density to $0.055 \times 10^{-4}\,\mathrm{nm}^{-2}$ indicate effective lattice stabilization. At the microstructural scale, feature analysis reveals a fourfold increase in the number of resolved sub-grains (10,485), reflecting a more homogeneous ferritic matrix. Importantly, these changes occur alongside only a moderate decrease in microhardness, from 225.43 HV in the as-received state to 208.22 HV after annealing.

Overall, this multi-scale analysis demonstrates that annealing at 200 ℃ reduces defect density and enhances structural uniformity while avoiding the grain growth and mechanical softening typically associated with higher-temperature treatments.

3.6. Computational microstructural informatics and recovery efficiency mapping

To establish a consistent connection between different scales of analysis, a computational framework was developed using Python-based tools. This framework integrates lattice-scale information from XRD, microstructural observations from SEM, and macroscopic mechanical data from Vickers hardness measurements. By combining these datasets, a multi-scale "fingerprint" of the material is obtained, enabling a quantitative tracking of the static recovery process.

A central feature of this framework is the estimation of stored energy (E_s), representing the energy retained in the lattice due to the dislocation density (ρ) generated during TMCP. The stored energy per unit volume was calculated using a dislocation-based relation [9, 14]:

$$E_\mathrm{s} = \alpha \rho G b^2, \tag{5}$$

where α is a geometric factor (0.5 for ferritic BCC steel), G is the shear modulus of X70 steel (80 GPa), and b is the Burgers vector (0.248 nm). This approach provides a physically meaningful assessment of the effect of annealing at 200 ℃. The observed reduction in stored energy, together with the decrease in lattice microstrain and the moderate change in hardness, indicates that the material achieves a stable recovery state while maintaining its mechanical integrity. Overall, the computational framework integrates the experimental observations into a coherent description of the microstructural evolution.

3.6.1. Computational synthesis of microstructural fingerprint evolution

To assess the effect of isothermal annealing at 200 ℃ on API 5L X70 steel, a multi-scale "fingerprint" was generated using a Python-based radar mapping approach (Fig. 6). This method combines normalized

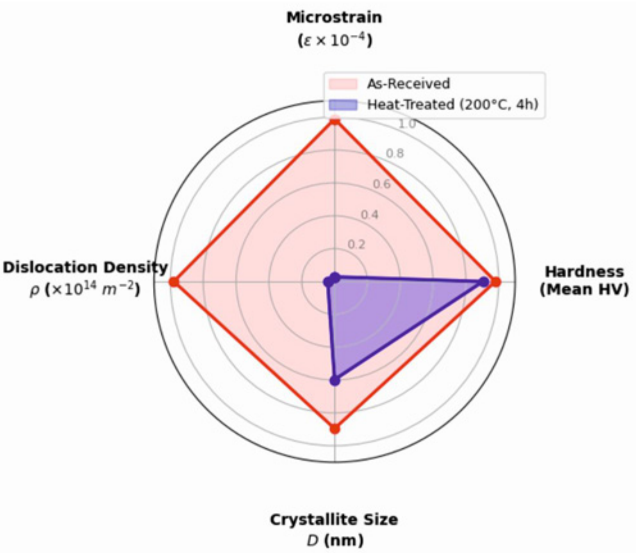

Fig. 6. Multi-scale "fingerprint" evolution: A Radar Map correlating crystallographic parameters (XRD) and mechanical hardness for API 5L X70 steel.

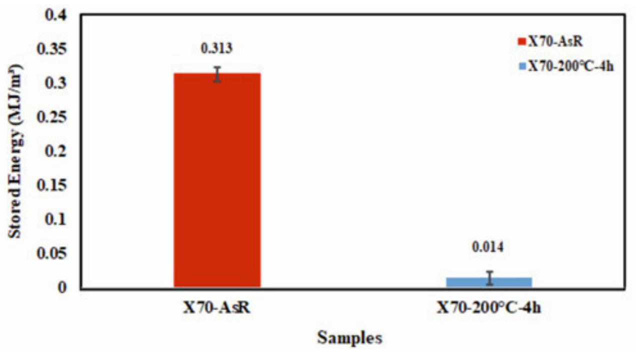

Fig. 7. Calculated stored energy reduction based on dislocation density evolution for API 5L X70 steel.

crystallographic parameters from XRD with macroscopic mechanical data, revealing a clear trend toward substructure relaxation. The contraction of the microstrain and dislocation density axes indicates a substantial reduction in internal lattice defects.

The results show that lattice microstrain decreases by approximately 97 %, while the average Vickers hardness is only moderately reduced by about 7.6 %. This demonstrates that the thermal treatment effectively promotes dislocation rearrangement and partial annihilation without causing grain coarsening or significant softening. Overall, the integrated radar representation supports a recovery-dominated mechanism, where the material reaches a more stable structural state while maintaining its mechanical integrity and load-bearing capacity.

3.6.2. Thermodynamic analysis of stored energy release

To further clarify the thermodynamic basis of the observed recovery, the stored energy (E_s) associated with the dislocation network was evaluated (Fig. 7). The results show a significant reduction in internal energy, from 0.313 MJ m^{-3} in the as-received condition to 0.014 MJ m^{-3} after isothermal annealing at 200 ℃. This large decrease – over 95 % of the initial stored energy – provides the main driving force for the nearly complete relaxation of lattice microstrain observed in the XRD data.

Mechanistically, this indicates that thermal activation at 200 ℃ is sufficient to enable dislocation movement and partial annihilation of defects, leading to stabilization of the ferritic matrix. Importantly, this substantial energy reduction occurs alongside only a modest decrease in hardness, as confirmed by the multi-scale radar analysis. The mild annealing thus transforms the material from a high-energy, metastable state to a more stable configuration, relieving internal stresses without causing softening or recrystallization. As a result, the steel preserves its mechanical integrity and suitability for long-term pipeline service.

3.6.3. Quantitative evaluation of recovery efficiency and multi-scale response

To assess the effectiveness of the 200 ℃ annealing treatment, a Recovery Efficiency Map was constructed (Fig. 8). The analysis shows a highly efficient recovery: lattice microstrain decreased by 97.1 %, indicating almost complete stress relaxation, while the macroscopic hardness dropped only slightly by 7.6 %. This demonstrates that the applied thermal cycle effectively promotes static recovery – mainly through the rearrangement and partial annihilation of dislocations – without reaching the conditions that would lead to full recrystallization or significant grain growth.

From an engineering standpoint, this balance is particularly beneficial for API 5L X70 pipeline steel, as it restores internal structural stability while preserving load-bearing capacity and overall mechanical performance. By combining atomic-scale stress relief with macroscopic mechanical stability and visualizing the results through Python-based statistical mapping, this approach offers a practical framework for optimizing low-temperature heat treatments in microalloyed steels.

4. Conclusions

This study presents a comprehensive multi-scale framework for investigating the microstructural and

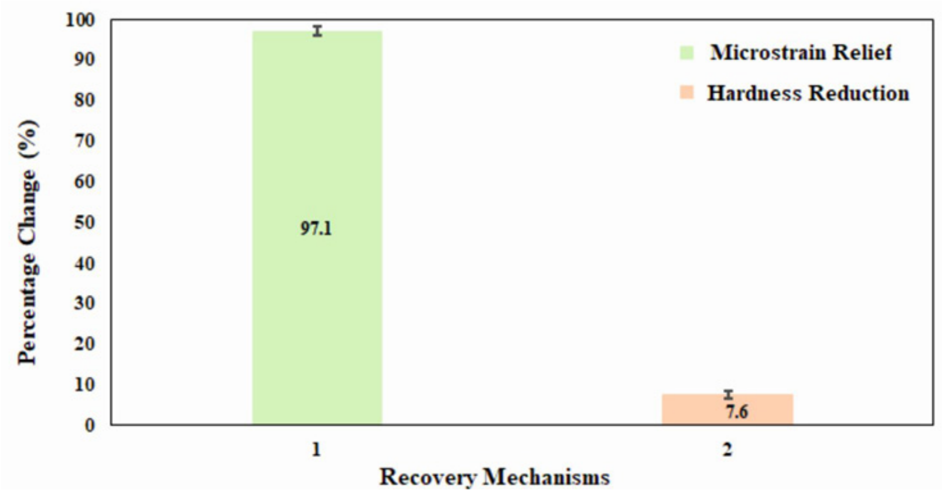

Fig. 8. Recovery efficiency map for API 5L X70 steel illustrating the disproportionate relationship between internal microstrain relaxation and macroscopic mechanical softening after 200 ℃ annealing.

mechanical evolution of API 5L X70 steel under low-temperature annealing. By integrating X-ray diffraction, electron microscopy, and computational modeling, the main findings can be summarized as follows:

– *Thermodynamic stabilization and energy dissipation*: Isothermal annealing at 200 ℃ for 4 h effectively relieves internal stresses. The lattice microstrain decreased from 6.53×10^{-4} to 0.19×10^{-4}, while the stored energy dropped from 0.313 to 0.014 $\mathrm{MJ\,m^{-3}}$, indicating a transition from a high-energy metastable state toward a more thermodynamically stable configuration.

– *Dominance of static recovery:* Crystallographic and morphological analyses confirm that static recovery is the dominant mechanism. Dislocations progressively rearrange into stable sub-boundaries, which preserves the ferritic matrix and prevents significant grain growth or the formation of new grains.

– *Microstructural homogenization:* Quantitative analysis reveals a fourfold increase in resolved subgrain features (up to 10,485 units) accompanied by a marked reduction in mean projected area. This reflects a more homogeneous microstructure, which is essential for consistent mechanical performance along pipeline sections.

– *Mechanical performance and recovery efficiency:* Annealing at 200 ℃ achieves a favorable balance between stress relief and strength retention. The Recovery Efficiency Map indicates a 97.1 % reduction in microstrain with only a 7.6 % decrease in Vickers hardness (208.22 HV), ensuring the preservation of load-bearing capacity.

– *Multi-scale validation via computational analysis:* The Python-based "fingerprint" framework shows strong correlations between lattice-scale defects and macroscopic properties. This confirms that the mechanical response is primarily governed by dislocation rearrangement and relaxation of internal elastic fields rather than grain coarsening.

– *Study limitation and future work:* Although only one annealing temperature (200 ℃) was investigated, this choice was intentional to isolate the effect of mild thermal exposure on dislocation rearrangement without triggering phase transformations or recrystallization phenomena. Future work will extend the study to a broader range of temperatures and holding times to further optimize the recovery process and clarify the transition between recovery and recrystallization mechanisms.

These findings highlight that low-temperature annealing at 200 ℃ provides an efficient and reliable industrial route for in-situ stress relief. The treatment mitigates residual stresses, limits degradation mechanisms, and preserves mechanical strength, thereby contributing to the extended service life of critical energy infrastructure.

Acknowledgement

The authors would like to express their sincere gratitude to Mohamed Khider University of Biskra for its generous support and for providing the essential facilities and resources that played a vital role in the successful completion of this research.

References

[1] K. Digheche, Z. Boumerzoug, M. Diafi, K. Saadi, Influence of heat treatments on the microstructure of welded API X70 pipeline steel, Acta Metall. Slovaca 23 (2017) 72–78. https://doi.org/10.12776/ams.v23i1.879
[2] L. R. Jacobo, R. García-Hernández, V. H. López-Morelos, A. Contreras, Effect of acicular ferrite and

bainite in API X70 steel obtained after applying a heat treatment on corrosion and cracking behaviour, Met. Mater. Int. 27 (2021) 3750–3764. https://doi.org/10.1007/s12540-020-00805-7
[3] J. W. Marian Domanski, A review of heat treatment research, Lithic Technol. 32 (2007) 153–194. https://doi.org/10.1080/01977261.2007.11721052
[4] B. C. Acosta-Cinciri, N. M. López-Granados, J. A. Ramos-Banderas, C. A. Hernández-Bocanegra, P. Garnica-González, J. A. López-Corpus, Effect of heat treatment on the microstructure and mechanical properties of a low-carbon X80 pipeline steel, Mater. Sci. Pol. 39 (2021) 103–112. https://doi.org/10.2478/msp-2021-0012
[5] S. Wu, D. Wang, Z. Zhang, C. Li, X. Liu, X. Meng, Z. Feng, Mechanical properties of low-transformation-temperature weld metals after low-temperature post-weld heat treatment, Sci. Technol. Weld. Join. 24 (2019) 112–120. https://doi.org/10.1080/13621718.2018.1492776
[6] R. Wang, Effects of hydrogen on the fracture toughness of a X70 pipeline steel, Corros. Sci. 51 (2009) 2803–2810. https://doi.org/10.1016/j.corsci.2009.07.013
[7] V. D. Mote, Y. P. Purushotham, B. N. Dole, Williamson-Hall analysis in estimation of lattice strain in nanometer-sized ZnO particles, J. Theor. Appl. Phys. 6 (2012) 6.
[8] G. K. Williamson, W. H. Hall, X-ray line broadening from filed aluminium and wolfram, Acta Metall. 1 (1953) 22–31. https://doi.org/10.1016/0001-6160(53)90006-6
[9] G. K. Williamson, R. E. Smallman, III. Dislocation densities in some annealed and cold-worked metals from measurements on the X-ray debye-scherrer spectrum, Philos. Mag. 1, (1956) 34–46. https://doi.org/10.1080/14786435608238074
[10] Z. Wang, U. Garbe, H. Li, Y. Wang, A. J. Studer, G. Sun, R. P. Harrison, X. Liao, M. A. Vicente Alvarez, J. R. Santisteban, C. Kong, Microstructure and texture analysis of δ-hydride precipitation in Zircaloy-4 materials by electron microscopy and neutron diffraction, Appl. Crystallogr. 47 (2014) 303–315. https://doi.org/10.1107/S1600576713031956
[11] B. D. Cullity, S. R. Stock, Elements of X-Ray Diffraction, 3rd ed., Prentice Hall. Upper Saddle River, New York, 2001, p. 388. ISBN-10: 0201610914.
[12] D. Balzar, X-ray diffraction line broadening: modeling and applications to high-Tc superconductors, J. Res. Natl. Inst. Stand. Technol. 98 (1993) 321–353. https://doi.org/10.6028/jres.098.026
[13] H. P. Klug, L. E. Alexander, X-Ray Diffraction Procedures for Polycrystalline and Amorphous Materials, 2nd ed., John Wiley and Sons, New York, 1974, pp. 618–708. ISBN: 978-0-471-49369-3.
[14] T. Ungár, Microstructural parameters from X-ray diffraction peak broadening, Scr. Mater. 51 (2004) 777–781. https://doi.org/10.1016/j.scriptamat.2004.05.007
[15] E. A. Little, The physical metallurgy of microalloyed steels, Mater. Sci. Technol. 16 (2000) p. 941.
[16] C. Ma, L. Guo, H. Li, W. Tan, T. Duan, N. Liu, M. Zhang, Effects of high-temperature annealing on the microstructures and mechanical properties of C/C–ZrC–SiC composites prepared by precursor infiltration and pyrolysis, Mater. Des. 90 (2016) 373–378. http://dx.doi.org/10.1016/j.matdes.2015.10.140
[17] I. Z. Awan, Recovery, recrystallization, and grain-growth, J. Chem. Soc. Pakistan 41 (2019) 1–42. https://doi.org/10.52568/000707/JCSP/41.01.2019
[18] J. I. Langford, A. J. C. Wilson, Scherrer after sixty years: a survey and some new results in the determination of crystallite size, Appl. Crystallogr. 11 (1978) 102–113. https://doi.org/10.1107/S0021889878012844
[19] W. H. Y. Zhao, S. Zhang, Effect of welding speed on microstructure, hardness and tensile properties in laser welding of advanced high strength steel, Sci. Technol. Weld. Join. 18 (2013) 581–590. https://doi.org/10.1179/1362171813Y.0000000140
[20] L. Longfei, Y. Wangyue, S. Zuqing, Dynamic recrystallization of ferrite in a low-carbon steel, Metall. Mater. Trans. A 37 (2006) 609–619. https://doi.org/10.1007/s11661-006-0033-y
[21] Z. Sami, A. Omar, Effects of the tempering temperature on microstructure and mechanical properties of X70 dual phase steel, Metall. Mater. Eng. 28 (2022) 351–358. https://doi.org/10.30544/753
[22] D. Liu, Y. Dong, R. Li, J. Jiang, X. Li, Z. Wang, X. Zuo, Evaluation of mechanical properties and microstructure of X70 pipeline steel with strain-based design, Metals 12 (2022) 1616. https://doi.org/10.3390/met12101616
[23] T. Zhu, C. Miao, Z. Cheng, Z. Wang, Y. Cui, F. Li, Effect of annealing process on the mechanical properties of X70 pipeline steel, MATEC Web of Conferences 186 (2018) 02001. https://doi.org/10.1051/matecconf/201818602001
[24] M. A. Mohtadi-Bonab, J. A. Szpunar, L. Collins, R. Stankievech, Evaluation of hydrogen induced cracking behavior of API X70 pipeline steel at different heat treatments, Int. J. Hydrogen Energy 39 (2014) 6076–6088. https://doi.org/10.1016/j.ijhydene.2014.01.138
[25] M. Masoumi, C. C. Silva, H. F. G. de Abreu, Effect of rolling in the recrystallization temperature region associated with a post-heat treatment on the microstructure, crystal orientation, and mechanical properties of API 5L X70 pipeline steel, Mater. Res. 20 (2017) 151–160. http://dx.doi.org/10.1590/1980-5373-MR-2016-0651